Materials Chemistry and Physics xxx (2009) xxx–xxx

Contents lists available at ScienceDirect

Materials Chemistry and Physics

journal homepage: www.elsevier.com/locate/matchemphys

Synthesis, characterization and photoluminescence properties of Dy^{3+}-doped nano-crystalline SnO_2

Sreejarani K. Pillai [a], Lucky M. Sikhwivhilu [a], Thembela K. Hillie [a,b,*]

[a] National Centre for Nano-Structured Materials, CSIR, PO Box 395, Pretoria 0001, South Africa
[b] Physics Department, University of the Free State, P.O. Box 339, Bloemfontein 9300, South Africa

ARTICLE INFO

Article history:
Received 9 May 2009
Received in revised form 9 December 2009
Accepted 11 December 2009

Keywords:
Dy^{3+}-doped SnO_2
Characterization
Photoluminescence

ABSTRACT

Nano-crystalline of tin oxide doped with varying wt% of Dy^{3+} was prepared using chemical co-precipitation method and characterised by various advanced techniques such as BET-surface area, Fourier transform infrared spectroscopy, X-ray diffraction, Raman spectroscopy and photoluminescence measurements. Analytical results demonstrated that the nanocrystalline tin oxide is in tetragonal crystalline phase and doping with Dy^{3+} could inhibit the phase transformation, increases surface area and decreases the crystallite size. The experimental result on photoluminescence characteristics originating from Dy^{3+}-doping in nanocrystalline SnO_2 reveals the dependence of the luminescent intensity on dopant concentration.

1. Introduction

Rare earth (RE)-doped nanoparticles have been attracting recently special attention due to their interesting physical properties, different than bulk materials, with applications in high brightness displays, laser emitters, fluorescent markers, thin-film electroluminescent (TFEL) devices, etc. [1]. In TFEL devices, luminescent properties are related to the intra-4f rare-earth transition [2,3], because their transitions take place in a wide energy range, with emissions from the visible to the infrared, allowing their application in several kinds of optical communication devices. In case of rare-earth ions, the electronic f–f transitions involve electrons which are localized in atomic orbital of the ions. Therefore, no size-dependent quantization effect from confinement of delocalized electrons is found of these transitions. However, confinement effects of semiconductor nanoparticles create photogenerated carriers may have an interaction with f-electrons which has important manifestations in influencing the optical properties. Thus, a nanostructure controls either by judiciously choosing the nanoenvironment of the species to be excited or by utilizing a nanoconfined structure that can be utilized to manipulate the excitation dynamics. Nanoscopic interactions play key roles in controlling the excitation dynamics. The efficiency of a nanomaterial is often limited by the band-to-band recombination and non-radiative surface recombination rates [4]. Transparent oxide semiconductors are being investigated as a matrix for the incorporation of these rare-earth ions, due to a high transparency in the visible, which when allied to rare-earth emission may contribute to the development of new technologies. Since the publication of Bhargava et al. [5] where they show strong orange luminescence from Mn^{2+} ions-doped ZnS nanoparticles, there are many reports on the optical properties of the ions-doped nanoparticles because a quantum confinement effect of carriers can be created.

Tin oxide (SnO_2), an n-type semiconductor with a wide band gap (E_g = 3.6 eV at 300 K), is extensively used as a functional material for optoelectronic devices [6], conductive electrodes and transparent coatings due to its good conductivity and transparency in the visible spectrum [7,8], solar cells [9,10], and catalyst support [11]. The variation of grain size, the concentration of oxygen vacancies and electrical properties of tin oxide as bulk as well as forms of thin films are also widely studied. A large number of research works have been focused on the electrical properties of SnO_2, especially for sensor and catalyst. Whereas, only a small amount of work is devoted to the luminescence properties of SnO_2, namely SnO_2-based phosphors. Compared with other traditional dielectric host materials, its good electrical conductivity together with high transparency at the visible and near-infrared wavelengths can be useful for developing new material combinations capable of emitting photons *via* electroluminescence as well as photoluminescence.

Dy^{3+} ion has two dominant bands in the emission spectrum. The yellow band (575 nm) corresponds to the hypersensitive transition $^4F_{9/2}$–$^6H_{13/2}$ ($\Delta L = 2$, $\Delta J = 2$), and the blue band (480 nm) corresponds to the $^4F_{9/2}$–$^6H_{15/2}$ transition. These hypersensitive transition relative intensities can be regulated by acting on

* Corresponding author at: Tel.: +27 12 841 3874; fax: +27 12 841 2229.
E-mail address: thillie@csir.co.za (T.K. Hillie).

0254-0584/$ – see front matter © 2009 Elsevier B.V. All rights reserved.
doi:10.1016/j.matchemphys.2009.12.010

Table 1
Surface area and pore volume of pure and Dy^{3+}-doped SnO_2.

Sample	BET surface area ($m^2\ g^{-1}$)	Pore volume ($cm^3\ g^{-1}$)
Pure SnO_2	29.87	0.0768
Dy-1	39.56	0.0972
Dy-2	42.58	0.0932
Dy-3	45.77	0.0891
Dy-4	49.53	0.0933

factors like the excitation wavelength, the host composition and the doping concentration [12–15]. Hence it is important to understand local structural environments and spatial distribution of dopants when developing a nano-sized luminescent material activated by RE elements because absorption and emission properties of intra-4f-configurational transitions of RE ions are sensitive to their chemical and structural status in a host matrix [13].

Based on the above considerations, in this study, we have aimed at fabrication of Dy^{3+}-doped nanocrystalline tin oxide by a chemical co-precipitation route. This method has been employed quite frequently to synthesize nanoparticles because of its low cost and good stoichiometric control. The structural and luminescence properties of the pure and doped systems are investigated.

2. Experimental

The precipitate of pure SnO_2 was obtained by adding NH_4OH solution and $SnCl_4{\cdot}5H_2O$ solution with stirring until the pH of mother liquid was 10. The precipitate was coagulated for 15 min and allowed to stand overnight. The precipitate was filtered, washed until the solution was free from Cl^- ions. The precipitate obtained was oven dried at 383 K for 12 h, powdered and calcined at 773 K for 6 h.

A typical chemical co-precipitation technique was used to prepare the rare earth (0.2, 0.5, 1 and 2 wt% designated as Dy-1, Dy-2, Dy-3 and Dy-4 respectively) doped samples. $SnCl_4{\cdot}5H_2O$ (5 g) and required amount of Dy $(NO_3)_3{\cdot}5H_2O$ were dissolved in 250 ml distilled water. Under stirring with a magnetic stirrer, NH_4OH was added drop wise until the pH reached 10. The precipitate obtained was submitted to dialysis against distilled water along with centrifugation several times to eliminate Cl^-, NO_3^- and NH_4^+ ions (until the supernatant solution showed no precipitation for the tests for Cl^-, NO_3^- and NH_4^+ ions). The precipitate obtained was oven dried at 383 K for 12 h, powdered and calcined at 773 K for 6 h.

Simultaneous determination of BET (Brunauer, Emmett, and Teller) surface area and total pore volume of the samples were achieved in a Micromeritics TRISTAR 3000 surface area analyzer by the low temperature N_2 adsorption method. Prior to analysis, the samples were degassed at 120 °C overnight (12 h) under a continuous flow of N_2 gas to remove adsorbed contaminants from the surface and pores of the CNTs. The crystalline phases of the samples were determined by X-ray diffraction (PAnalytical XPERT-PRO diffractometer) measurement, using Fe filtered Co Kα radiation (λ = 1.789 Å), with variable slit at 35 kV, 50 mA. FT-IR spectra of the samples were recorded using a Perkin Elmer Spectrum 100 spectrometer attached with an FT-IR Microscope accessory, equipped with a germanium crystal. Background was run before the analysis and all the spectra were baseline corrected. Raman spectra of pure and doped samples were recorded by Lab Raman system (Jobin-Yvon Horiba T64000 Spectroscopy) equipped with an Olympus BX-40 microscope. The excitation wavelength was of 514.5 nm with an energy setting of 1.2 mW from a Coherent Innova Model 308 argon ion laser. The surface morphology of the powder samples was studied by FE-SEM (JEOL 7500F SEM). Both fluorescence excitation and emission spectra were recorded at room temperature on Perkin Elmer LS-55 fluorescence spectrometer. The excitation source was 75 W Xenon lamp and the spectral resolution was 1 nm. The TEM analysis was done on a JEOL 2100 F TEM operated at an accelerating voltage of 100 kV. Powder sample was sonicated in methanol for 10 min, a drop of which was deposited on a holey carbon film coated Cu-grid.

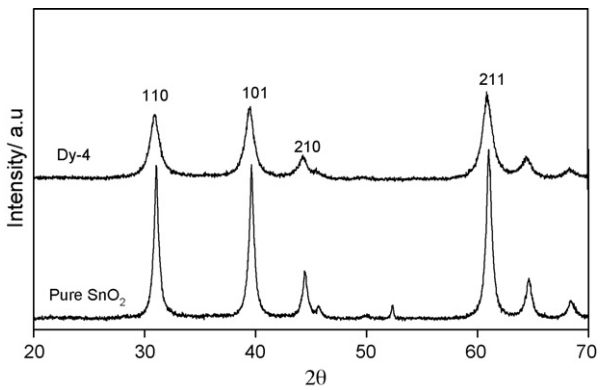

Fig. 1. XRD patterns of pure and Dy^{3+}-doped (2 wt%) SnO_2 samples calcined at 773 K.

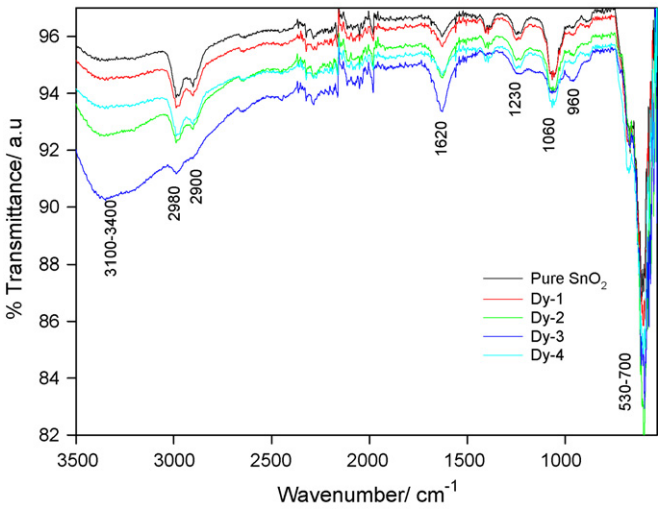

Fig. 2. FTIR spectra of pure and Dy^{3+}-doped SnO_2 samples.

3. Results and discussion

The BET specific surface areas of the Dy-doped samples calcined at 823 K were in the range of 39–49 $m^2\ g^{-1}$ (see Table 1). The addition of small amount of dopant caused the doped system to show smaller particle size and higher surface area compared to the pure system and the reduction in grain size was gradual with Dy^{3+} content. This increase may be due to the formation of Dy–Sn composite oxide, which effectively hinder the boundary mobility and hence the grain growth [14,15].

The powder X-ray diffractograms of the pure, Dy-doped sample (2 wt%) calcined at 773 K are given in Fig. 1. The sharp peaks in the XRD pattern of pure tin oxide show that it is highly crystalline and the position of the peaks reveals that SnO_2 is in tetragonal rutile phase. Broadening of diffraction peaks can be observed, in the doped sample implying the reduction in crystallite size. The absence of the known crystalline phases of Dy_2O_3 in the sample suggests that the dopant is well dispersed in the host SnO_2 material.

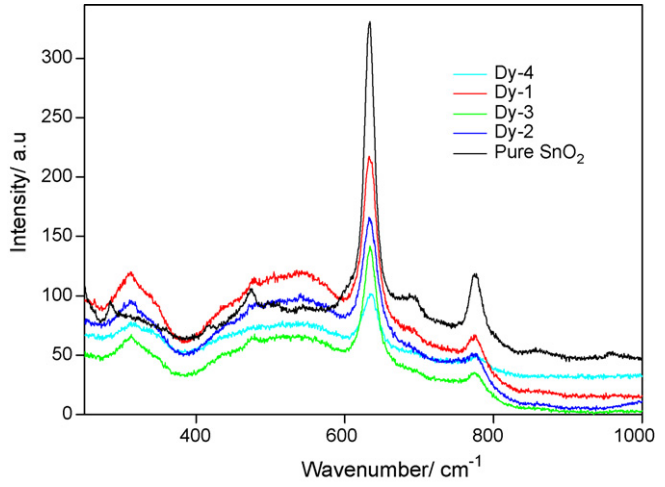

Fig. 3. Raman spectra of pure and Dy^{3+}-doped SnO_2 samples.

Please cite this article in press as: S.K. Pillai, et al., Synthesis, characterization and photoluminescence properties of Dy^{3+}-doped nano-crystalline SnO_2, Mater. Chem. Phys. (2010), doi:10.1016/j.matchemphys.2009.12.010

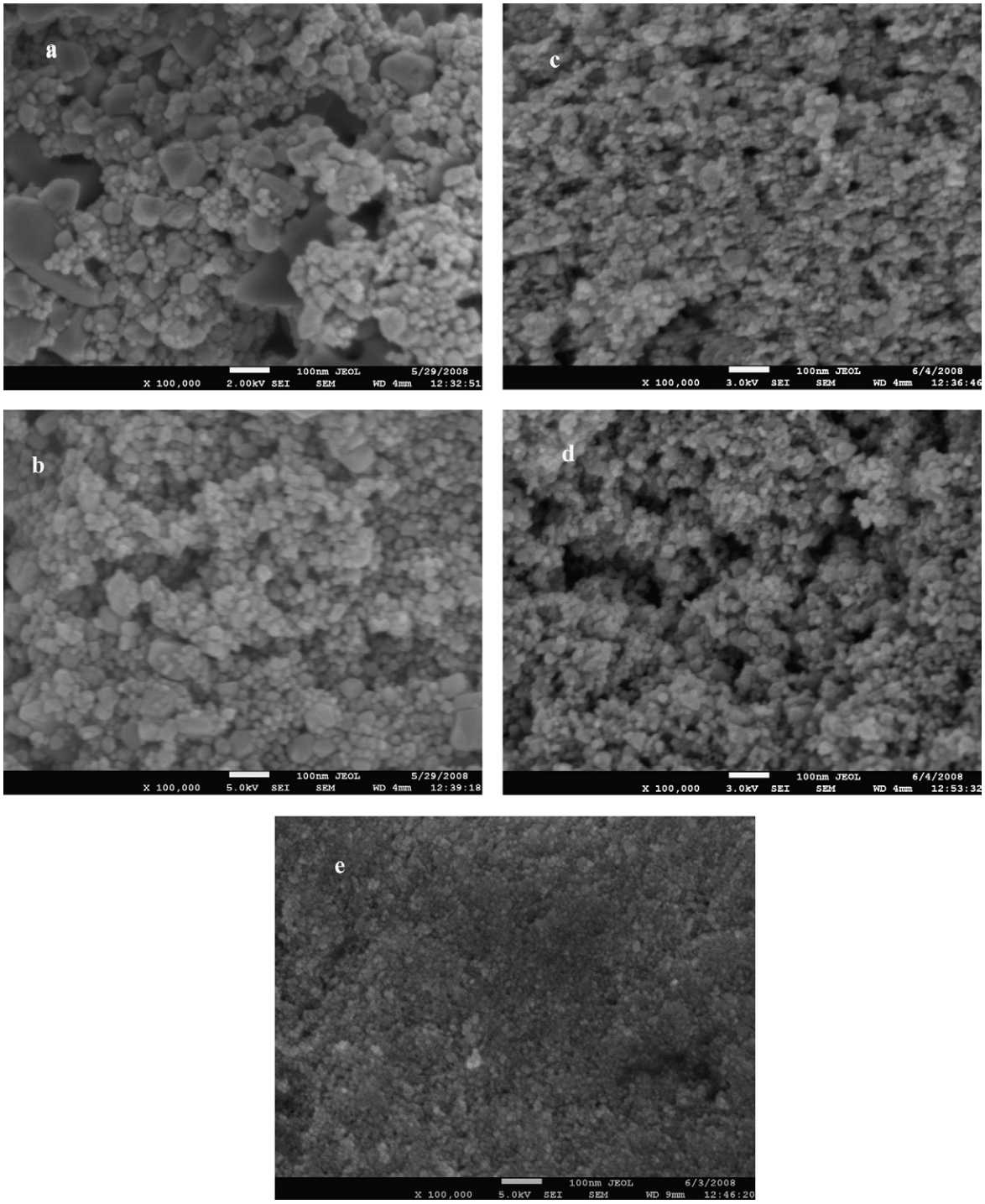

Fig. 4. SEM micrographs of pure and Dy^{3+}-doped SnO_2 samples (a) pure, (b) Dy-1, (c) Dy-2, (d) Dy-3, and (e) Dy-4.

The FT-IR transmittance spectra of different samples are given in Fig. 2. The broad absorption band between 3100 and 3400, the peaks at 1620 and 1230 cm^{-1} are attributed to vibration of hydroxyl groups associated with structural water [16]. The bands at 2980 and 2900 cm^{-1} are assigned to C–H vibrations which could be attributed to the organic trace impurities, which were incorporated during calcination process. The bands observed in the range of 1060 and 970 cm^{-1} are due to the vibration of Sn=O and Sn–O surface cation-oxygen bonds [17]. The typical M–O–M (in this case Sn–O–Sn) vibrations appear in the range of 530–700 cm^{-1} [18]. No additional absorption peaks were observed with Dy^{3+}-addition, indicating its homogeneous dispersion in the support material.

Fig. 3 shows the Raman spectra of pure and Dy-doped samples calcined at 823 K. Pure SnO_2 shows three prominent Raman peaks at 476, 633 and 774 cm^{-1} which are assigned to E_g, A_{1g} and B_{2g} modes respectively [19]. All these Raman features confirm the tetragonal rutile structure for the SnO_2 sample. The broad peak around 350 cm^{-1} which was reported in extra-fine (3–5 nm) nanoparticles [20,21] is observed in all the doped samples. This

Please cite this article in press as: S.K. Pillai, et al., Synthesis, characterization and photoluminescence properties of Dy^{3+}-doped nano-crystalline SnO_2, Mater. Chem. Phys. (2010), doi:10.1016/j.matchemphys.2009.12.010

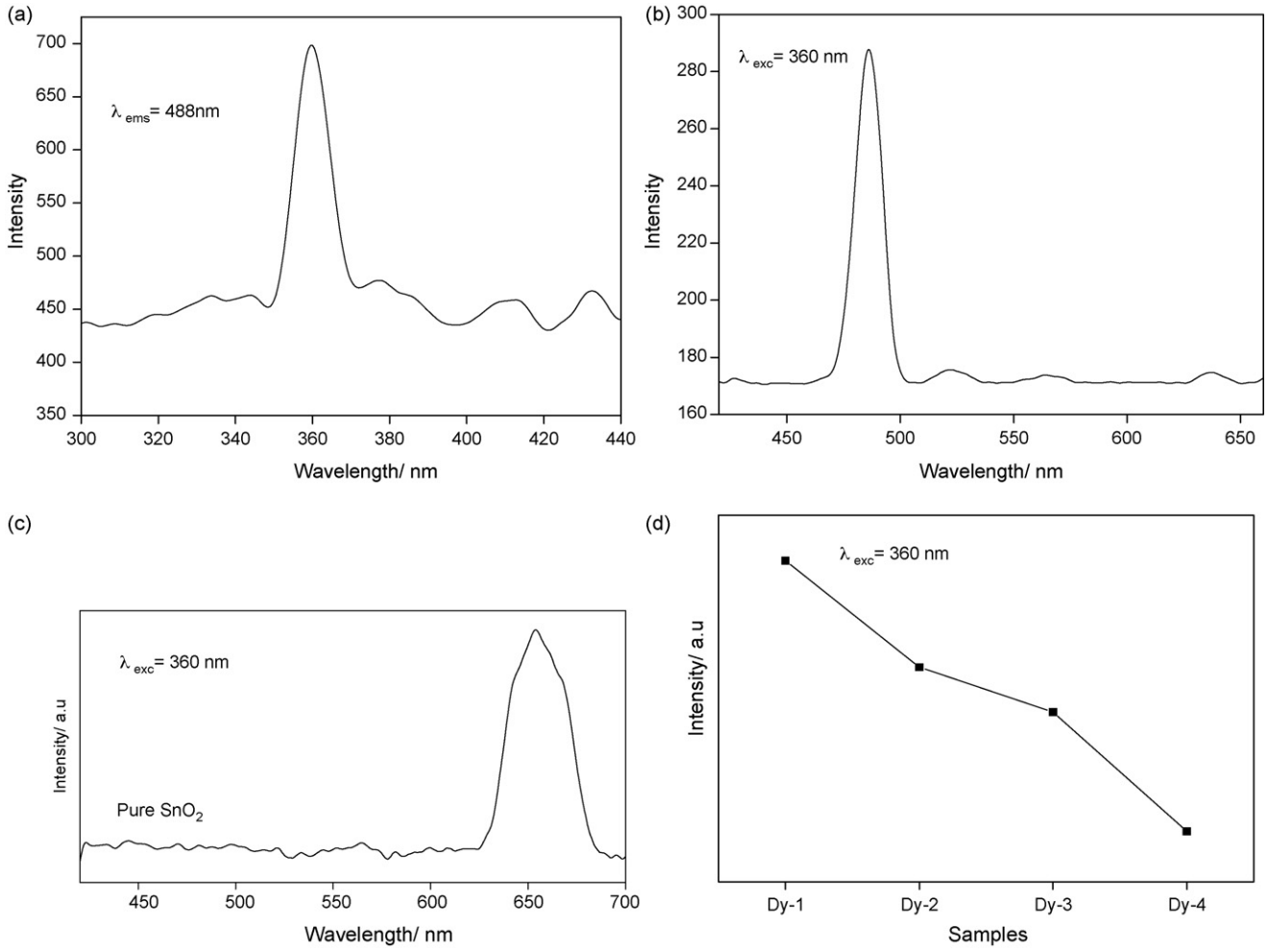

Fig. 5. PL spectra of pure and Dy^{3+} -doped SnO_2 samples recorded at room temperature (a) excitation spectrum of Dy-1 (b) emission spectrum of pure SnO_2 (c) emission spectrum of Dy-1 (d) emission intensity vs. concentration of various Dy^{3+} -doped SnO_2 samples (λ_{max} = 580 nm).

attributes to relaxation of Raman selection rule by reduction in the particle size or by the high concentration of surface defects such as oxygen vacancies and lattice disorder [22]. Another feature to be noted is the decrease in A_{1g} mode intensity in the doped samples. The decrease in the intensity suggests that the dopant interacts strongly with the support and is probably covering the SnO_2 grains with monolayer. The interaction between the Dy^{3+} atoms and the support oxide hinders the crystallization, which is reflected in the reduction of peak intensity. The absence of the known crystalline phases of Dy_2O_3 in the doped samples suggests that it is finely dispersed in SnO_2 matrix. This observation supports BET, XRD and FTIR results.

The typical morphology of the pure and Dy^{3+}-doped SnO_2 samples after calcination at 773 K is shown in Fig. 4a–e. All the images showed the presence of porous aggregates composed of smaller individual particles. The particle size ranges obtained from the SEM data were 24–121 nm (Pure), 19–99 nm (Dy-1), 16–68 nm (Dy-2), 10–38 nm (Dy-3) and 4–21 nm (Dy-4) respectively. It is thus clear that on incorporation of Dy^{3+}, the particle size of SnO_2 reduces suggesting that the dopant influences the grain growth of SnO_2 material. The reduction in particle size is quite gradual with dopant concentration which is in agreement with BET surface area results. The higher grain growth inhibition could be attributed to the increased nucleation sites resulting from higher stacking fault energy due to Dy^{3+} addition to the pure material [23].

The excitation spectrum in Fig. 5a is the scanning of excited wavelength from 300 to 440 nm when the emission wavelength was set at 488 nm, for the sample with 2 wt% of Dy^{3+} content. The excitation maxima for the 488 nm emission is located at 360 nm corresponding to the transition from the ground level $^6H_{15/2}$ to the hypersensitive level $^6P_{7/2}$, from where it relaxes non-radiatively to the $^4F_{9/2}$ metastable level. The general observed peaks distribution agrees well with the reported structure distribution spectra for Dy^{3+} doped nanocrystalline ZrO_2 [24,25]. The PL spectrum acquired for pure SnO_2 (see Fig. 5b) consisted of broad red-green band peaked at about 650 nm.

The experimental results in Fig. 5c show the fluorescence emission from 400 to 650 nm of the pure and Dy^{3+}-doped SnO_2 (Dy-1) samples calcined at 773 K, under excitation at 360 nm. The strongest emission band was observed in the blue region centred at 488 nm ($^4F_{9/2}$–$^6H_{15/2}$) with a weak band in the yellow region centred at 580 nm ($^4F_{9/2}$–$^6H_{13/2}$) attributed to f–f transitions of Dy^{3+} in a solid solution and are very sensitive to the environment of the rare earth ion [26].

Gu et al. [27] reported the emission spectrum yields for sol–gel prepared Dy^{3+}-doped SnO_2 calcined at 673 K, which contained exclusively the characteristic emission lines of Dy^{3+}, peaking at 575 nm ($^4F_{9/2}$–$^6H_{13/2}$), and 658 nm ($^4F_{9/2}$–$^6H_{11/2}$). The hypersensitive transition ($^4F_{9/2}$–$^6H_{13/2}$ of Dy^{3+}) is dominant in the emission spectra resulting from the distorted crystal lattice at which Dy^{3+}

Please cite this article in press as: S.K. Pillai, et al., Synthesis, characterization and photoluminescence properties of Dy^{3+}-doped nano-crystalline SnO_2, Mater. Chem. Phys. (2010), doi:10.1016/j.matchemphys.2009.12.010

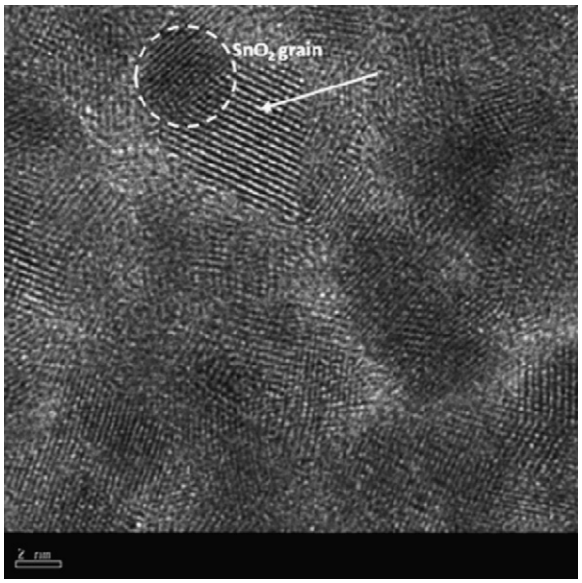

Fig. 6. HRTEM image of Dy^{3+}-doped (2 wt%) SnO_2.

ions locate. The emission spectrum of pure SnO_2 presented two bands centred at 400 and 430 nm, respectively. As the $^4F_{9/2}$–$^6H_{13/2}$ emission of Dy^{3+} belongs to hypersensitive transition with $\Delta J = 2$, which is strongly influenced by outside surroundings. When Dy^{3+} ion is located at a low symmetry local site (without an inversion centre), this emission transition is often prominent in its emission spectra [28].

In the present case the dominance of the magnetically allowed ($^4F_{9/2}$–$^6H_{15/2}$) transition for all the doped samples can be explained as follows. Since the radius of Dy^{3+} (0.91 Å) is larger than that of Sn^{4+} (0.76 Å), the host lattice will not easily accommodate Dy^{3+} and hence only a minor fraction of the total amount of Dy^{3+} introduced into the SnO_2 goes to the Sn-substitutional positions, most of the Dy^{3+} ions may well be precipitated into SnO_2:Dy^{3+} clusters. The excess Dy^{3+} phases will likely reside on the surface or on the grain boundaries of the nanoparticles to yield optimum strain relief which is evident from the TEM image (refer Fig. 6). Thus, in this case, the $^4F_{9/2}$–$^6H_{13/2}$ transition emission will not show prominent in the emission spectrum [27,29]. The difference in the emission characteristics in the samples may be due to the changes in the preparation conditions and calcination temperature.

Fig. 5d depicts the influence ofof Dy^{3+} concetration on the emission intensity of various Dy^{3+} doped SnO_2 samples. One can also observe that the highest emission corresponds to the 0.2 wt% Dy_2O_3 doped sample and concentration quenching of the Dy^{3+} luminescence is observed as Dy^{3+} concentration increases over 0.2 wt% Dy_2O_3. The quenching of the luminescence is best observed for the 2.0 wt% Dy_2O_3 doped sample. The most plausible explanation for such behaviour is cross-relaxation among Dy^{3+} pairs to the intermediate levels Dy^{3+} ($^6F_{3/2}$) and Dy^{3+} ($^6H_{9/2}$), from where the ions decay non-radiatively or by IR emission [30,31]. These quenching transitions are mainly Dy^{3+} ($^4F_{9/2}$) + Dy^{3+} ($^6H_{15/2}$) → Dy^{3+} ($^6F_{3/2}$) + Dy^{3+} ($^6H_{9/2}$). With increase in dopant concentration, most of Dy^{3+} ions may be absorbed at the SnO_2 grain surface, which offers much more opportunity for the cross-relaxation processes [29]. So for the Dy doped SnO_2 systems 0.2 wt% is found to be the optimum concentration for maximum Dy^{3+} luminescence.

4. Conclusions

Pure and Dy^{3+}-doped nanocrystalline SnO_2 were prepared by chemical co-precipitation method. Structural characterization of the samples using XRD, FTIR and Raman revealed tetragonal rutile phase for the host material. Dy^{3+} addition to pure SnO_2 increased the surface area and decreased the crystallite size. The emission spectra of the Dy^{3+}-doped samples showed characteristic $^4F_{9/2}$–$^6H_{15/2}$ emission and concentration quenching when the doping level was above the optimum concentration of 0.2 wt%.

Acknowledgement

Authors thank the Council for Scientific and Industrial Research executive and Department of Science and Technology, South Africa for the financial support.

References

[1] D.J. Norris, A.L. Efros, S.C. Erwin, Doped nanocrystals, Science 319 (2008) 1776–1779.
[2] H. Ennen, J. Schneider, G. Pomrenke, A. Axmann, 1.54-μm luminescence of erbium-implanted III–V semiconductors and silicon, Appl. Phys. Lett. 43 (1983) 943–945.
[3] S. Coffa, G. Franzo, F. Priolo, A. Polman, R. Serna, Temperature dependence and quenching processes of the intra-4*f* luminescence of Er in crystalline Si, Phys. Rev. B 49 (1994) 16313–16320.
[4] P.S. Chowdhury, S. Saha, A. Patra, Influence of nanoenvironment on luminescence of Eu^{3+}activated SnO_2 nanocrystals, Solid State Commun. 131 (2004) 785–788.
[5] R.N. Bhargava, D. Gallagher, X. Hong, A. Nurmikko, Optical properties of manganese-doped nanocrystals of ZnS, Phys. Rev. Lett. 72 (1994) 416–419.
[6] D.S. Kumar, P.R. Carbarrocas, J.M. Siefert, In situ investigation of theoptoelectronic properties of transparent conducting oxide/amorphous silicon interfaces, Appl. Phys. Lett. 54 (1989) 2088–2090.
[7] A. Lousa, S. Gimeno, J. Martı, Preparation conditions of transparent and conductive SnO_2 thin films by reactive evaporation, Vacuum 45 (1994) 1143–1145.
[8] A. Tsunashima, H. Yoshimizu, K. Kodaira, S. Shimada, T. Matsushita, Preparation and properties of antimony-doped SnO_2 films by thermal decomposition of tin 2-ethylhexanoate, J. Mater. Sci. 21 (1986) 2731–2734.
[9] S. Ferrere, A. Zaban, B.A. Gregg, Dye sensitization of nanocrystalline tin oxide by perylene derivatives, J. Phys. Chem. B 101 (1997) 4490–4493.
[10] Y. Tachibana, K. Hara, S. Takano, K. Sayama, H. Arkawa, Investigations on anodic photocurrent loss processes on dye sensitized solar cells: comparison between nanocrystalline SnO_2 and TiO_2 films, Chem. Phys. Lett. 364 (2002) 297–302.
[11] D. Wang, S. Wen, J. Chen, S. Zhang, F. Li, Microstructure of SnO_2, Phys. Rev. B 49 (1994) 14282–14285.
[12] W. Jia, W. Xu, I. Rivera, A. Perez, F. Fernandez, Effects of compositional phase transitions on luminescence of $Sr_{1-x}Ca_xTiO_3$:Pr^{3+}, Solid State Commun. 126 (2003) 153–157.
[13] P. Boutinaud, R. Mahiou, E. Cavalli, M. Bettinelli, Excited state dynamics of Pr^{3+} in YVO_4 crystals, J. Appl. Phys. 96 (2004) 4923–4929.
[14] E.R. Leite, A.P. Maciel, I.T. Weber, P.N. Lisboa-Filho, E. Longo, C.O. Paiva-Santos, et al., Development of metal oxide nanoparticles with high stability against particle growth using a metastable solid solution, Adv. Mater. 14 (2002) 905–908.
[15] R.J. Brook, Controlled grain growth, in: F.F.Y. Wang (Ed.), Ceramic Fabrication Process, Academic Press, New York, 1976, pp. 331–364.
[16] K. Hadjiivanov, A. Davydov, D. Klissurski, IR spectroscopy applied to surface chemistry of oxides, Kinet. Catal. 29 (1988) 161–167.
[17] S. Lenaerts, J. Roggen, G. Maes, FT-IR characterization of tin dioxide gas sensor materials under working conditions, Spectrochim. Acta A 51 (1995) 883–894.
[18] L.M. Fang, X.T. Zu, Z.J. Li, S. Zhu, C.M. Liu, W.L. Zhou, et al., Synthesis and characteristics of Fe^{3+}-doped SnO_2 nanoparticles *via* sol–gel–calcination or sol–gel–hydrothermal route, J. Alloys Comp. 454 (2008) 261–267.
[19] P.S. Peercy, B. Morosin, Pressure and temperature dependences of the Raman-active phonons in SnO_2, Phys. Rev. B 7 (1973) 2779–2786.
[20] C.H. Shek, G.M. Lin, J.K.L. Lai, Effect of oxygen deficiency on the Raman spectra and hyperfine interactions of nanometer SnO_2, Nanostruct. Mater. 11 (1999) 831–835.
[21] K.N. Yu, Y.H. Xiong, Y.L. Liu, C.S. Xiong, Microstructural change of nano-SnO_2 grain assemblages with the annealing temperature, Phys. Rev. B 55 (1997) 2666–2671.
[22] A. Dieguez, A. Ramano-Rodrigues, A. Vila, J.R. Morante, The complete Raman spectrum of nanometric SnO_2 particles, J. Appl. Phys. 90 (2001) 1550.
[23] S. Rani, S.C. Roy, M.C. Bhatnagar, Effect of Fe doping on the gas sensing properties of nano-crystalline SnO_2 thin films, Sens. Actuators B: Chem. 122 (2007) 204–210.
[24] X. Fu, S. Niu, H. Zhang, Q. Xin, Photoluminescence of Dy^{3+} ions in yttrium-stabilized zirconium oxide with different phases, Mater. Sci. Eng. B 129 (2006) 14–17.
[25] L.A. Diaz-Torres, E. De la Rosa, P. Salas, V.H. Romero, C. Angeles-Chaĭvez, Efficient photoluminescence of Dy^{3+} at low concentrations in nanocrystalline ZrO_2, J. Solid State Chem. 181 (2008) 75–80.

Please cite this article in press as: S.K. Pillai, et al., Synthesis, characterization and photoluminescence properties of Dy^{3+}-doped nano-crystalline SnO_2, Mater. Chem. Phys. (2010), doi:10.1016/j.matchemphys.2009.12.010

[26] G. Dominiak-Dzik, W. Ryba-Romanowski, M.N. Palatnikov, N.V. Sidorov, V.T. Kalinnikov, Dysprosium-doped $LiNbO_3$ crystal. Optical properties and effect of temperature on fluorescence dynamics, J. Mol. Struct. 704 (2004) 139–144.
[27] F. Gu, S.F. Wang, M.K. Lu, Y.X. Qi, G.J. Zhou, D. Xu, D.R. Yuan, Preparation and luminescence characteristics of nanocrystalline SnO_2 particles doped with Dy^{3+}, J. Crystal Growth 255 (2003) 357–360.
[28] M. Yu, J. Lin, Z. Zhang, J. Fu, S. Wang, H.J. Zhang, et al., Fabrication, patterning, and optical properties of nanocrystalline YVO_4:A (A = Eu^{3+}, Dy^{3+}, Sm^{3+}, Er^{3+}) Phosphor Films via sol–gel soft lithography, Chem. Mater. 14 (2002) 2224–2231.
[29] F. Gu, S.F. Wang, M.K. Lu, G.J. Zhou, S.W. Liu, D. Xu, D.R. Yuan, Effect of Dy^{3+} doping and calcination on the luminescence of ZrO_2 nanoparticles, Chem. Phys. Lett. 380 (2003) 185–189.
[30] W.Y. Shen, M.L. Pang, J. Lin, J. Fang, Host-sensitized luminescence of Dy3+ in nanocrystalline β-Ga_2O_3 prepared by a Pechini-type sol–gel process, J. Electrochem. Soc. 152 (2005) H25–H38.
[31] G. Tripathi, V.K. Rai, S.B. Rai, Spectroscopy and upconversion of Dy^{3+} doped in sodium zinc phosphate glass, Spectrochim. Acta A 62 (2005) 1120–1124.

Please cite this article in press as: S.K. Pillai, et al., Synthesis, characterization and photoluminescence properties of Dy^{3+}-doped nano-crystalline SnO_2, Mater. Chem. Phys. (2010), doi:10.1016/j.matchemphys.2009.12.010